Analysis of Threshold Characteristics of Short-Wavelength Semiconductor Lasers

Bangguo Wang, Shaoyang Tan, Li Zhou, Wuling Liu, Lihong Zhu, Guoliang Deng, and Jun Wang

***Abstract*—Existing high-power semiconductor lasers widely use asymmetric large cavity structures or designs with short cavity lengths to enhance device performance, inevitably increasing the device threshold current density and suppressing further improvement of device performance. We have utilized rate equations analysis to investigate the impact of threshold current density on the threshold characteristic temperature of GaAs-based laser diodes at short wavelengths. A simplified carrier escape model has been employed, which is more accurate compared to the classical model of thermal carrier emission. Compared to long-wavelength laser diodes, short-wavelength laser diodes exhibit higher temperature stability due to their smaller Auger recombination coefficients. Increased internal losses caused by carrier escape and decreased injection efficiency are the main reasons for the decrease in threshold characteristic temperature with increasing temperature. The increase in threshold significantly enhances carrier escape, leading to a decrease in the threshold characteristic temperature and an increase in sensitivity to temperature. Moreover, high thresholds limit the increase in the device's decoupling factor, causing a decrease in current inject efficiency and further degradation of device performance. By increasing the barrier height, carrier escape can be effectively suppressed, thereby enhancing device performance. The simulation results agree well with the experimental data of InAlGaAs laser diodes at a wavelength of 780 nm, accurately predicting the threshold characteristics of devices with different cavity lengths at various temperatures.**

***Index Terms*—Laser diodes, rate equations, GaAs, carrier escape.**

I. Introduction

In THE past 30 years, semiconductor lasers have made rapid advancements [1]. Taking 800 nm as an example, the single chip output power has exceeded 19 W, and the chip conversion efficiency has exceeded 71%[2], [3]. Currently, high-power semiconductor lasers widely adopt an asymmetric large optical cavity structure to improve the output power of the devices [4], [5]. By effectively reducing the optical density of the active region through quantum well shifting, the maximum output power of the device is increased [6]. At the same time, the asymmetric waveguide can effectively reduce internal losses and series resistance, thus improving power conversion efficiency. For high-efficiency devices, a design with a short cavity length is often adopted [7]. Shortening the cavity length can effectively enhance the mirror loss, thereby improving the external quantum efficiency and increasing the device's power conversion efficiency [8]. However, both the asymmetric optimization and the shortening of the cavity length inevitably increase the device's threshold current density and limit further improvement in device performance [5].

The increase of threshold current density will result in a greater likelihood of carrier escape from the active region and entry into the barrier, leading to an increase in carrier density within the barrier region. At the same time, internal losses increase and internal quantum efficiency decreases [5]. For semiconductor lasers used in pumping applications, it is often necessary for the device to operate under continuous current conditions to provide sufficiently high average power output [9], [10], [11]. In this case, the actual junction temperature of the device is much higher than the temperature of the heat sink. Under high temperature conditions, carrier escape in the device becomes more severe, ultimately leading to a rollover phenomenon that limits further power enhancement of the device. We can evaluate the temperature stability of the device by obtaining the characteristic temperature of the device through simple exponential fitting [5], [12].

$$I_{th}(T) = I_{th0} * exp\left(\frac{T}{T_0}\right) \tag{1}$$

This parameter has been widely recognized and applied over the past 50 years [12], [13]. At the same time, the use of characteristic temperature can predict the continuous operation performance of the device to a certain extent, helping us optimize the device [5]. However, the characteristic temperature of the device is not a constant value and is only applicable to a certain temperature range. It will decrease with increasing temperature [14], [15], [16]. The increase in threshold current density increases the escape of carriers, resulting in decreased temperature stability of the device. Studying the influence of threshold current density on device performance is a meaningful work that can help us understand the working mechanism of the device and make accurate predictions of its performance. This can help us optimize the device and further improve its operational performance [17].

Manuscript received 10 February 2024; accepted 19 February 2024. Date of publication 22 February 2024; date of current version 21 March 2024. This work was supported by the National Key Research and Development Program of China under Grant 2018YFB1107300 and Grant 2016YFB0402202. *(Corresponding author: Jun Wang.)*

Bangguo Wang, Wuling Liu, Lihong Zhu, and Guoliang Deng are with the College of Electronics and Information Engineering, Sichuan University, Chengdu 610065, China (e-mail: wangbangguo@stu.scu.edu.cn).

Shaoyang Tan and Li Zhou are with the Suzhou Everbright Photonics Company Ltd., Suzhou 215000, China (e-mail: shaoyang.tan@everbrightphotonics.com).

Jun Wang is with the College of Electronics and Information Engineering, Sichuan University, Chengdu 610065, China, and also with Suzhou Everbright Photonics Company Ltd., Suzhou 215000, China (e-mail: wjdz@scu.edu.cn).

Digital Object Identifier 10.1109/JPHOT.2024.3368428

© 2024 The Authors. This work is licensed under a Creative Commons Attribution 4.0 License. For more information, see https://creativecommons.org/licenses/by/4.0/

The characteristic temperature of semiconductor lasers has been widely studied [17], [18], [19], [20], [21]. Based on the working mechanism of semiconductor lasers, researchers analyze the influence of temperature on various aspects such as gain, internal loss, internal quantum efficiency, and the carrier recombination in quantum well. In previous studies, a fixed carrier lifetime was often used to estimate the carrier density of devices [22]. The obtained differential gain and transparency carrier density both show a significant temperature dependence. This is inconsistent with traditional theories that the temperature dependence of Fermi–Dirac distribution function is dominant effect, as carrier lifetime is related to spontaneous radiative recombination coefficient, which is temperature-dependent [18], [23]. In long-wavelength devices, due to severe Auger recombination, they have lower temperature stability [20]. However, for short-wavelength ($\lambda < 980$ nm) devices, the current of Auger recombination is relatively small due to the higher Auger activation energy [24], [25], [26]. Theoretically, when only spontaneous radiative recombination in quantum wells is considered, the device should have very high temperature stability, and its threshold characteristic temperature T_0 increases linearly with temperature [27]. At this time, an increase in internal loss caused by carrier escape and a decrease in internal quantum efficiency are the main reasons for the decrease in device temperature stability [24].

In this article, we study the temperature characteristics of semiconductor lasers using rate equations analysis. Rate equations are widely used to investigate the static and dynamic performance of optoelectronic devices [28], [29], [30]. Compared to light-emitting diodes and communication devices, we are particularly interested in the threshold current and its impact on the device's internal losses, internal quantum efficiency, and temperature characteristics. In the second section, we introduce the rate equations and the relevant parameter models. We neglect the temperature dependence of the differential gain and assume a linear relationship between the transparent carrier density and temperature [18], [31], [32]. We employ a simplified model for carrier escape in quantum wells, which is more accurate for narrow wells and low potential barriers compared to the classical thermal carrier escape model [33], [34]. We analyze the unclamping rate at different thresholds current density, which has been considered a constant value in previous studies, leading to above-threshold current-injection efficiency being significantly underestimated as a function of threshold and temperature [35], [36]. In the third section, we compare the simulation results with experimental data, and the optimized model accurately predicts the threshold temperature characteristics of devices with different cavity lengths, aiding in the analysis and optimization of the devices.

II. Theory

Here, we utilize the three-level rate equations model to analyze the temperature characteristics of the threshold of the device [36]. Due to its lower effective mass, electrons are more susceptible to carrier escape [29]. In this study, we only consider the escape and capture of electrons. The escape and capture mechanism of carriers is illustrated in Fig. 1. Electrons are introduced into the active region via the N-Waveguide layer, while carriers undergo escape. This escape leads to an increase in the electron density within the P-Waveguide, resulting in increased internal loss. The rate equations can be expressed as follows [35]:

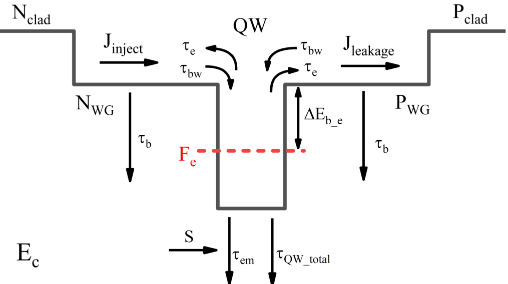

Fig. 1. Schematic diagram of carrier leakage and capture process in active region of quantum well laser.

$$\frac{N_{QW}}{dt} = \frac{N_B V_B}{\tau_{bw} V_{QW}} - N_{QW}\left(\frac{1}{\tau_{rad}} + \frac{1}{\tau_{nonrad}} + \frac{1}{\tau_e}\right) - \frac{v_g * S * g(N_{QW})}{1 + \varepsilon * S} \tag{2}$$

$$\frac{N_B}{dt} = \frac{I_{SCH}}{qV_B} - N_B\left(\frac{1}{\tau_b} + \frac{1}{\tau_{bw}}\right) + \frac{N_{QW} V_{QW}}{\tau_e V_B} \tag{3}$$

$$\frac{S}{dt} = \frac{\Gamma * v_g * S * g(N_{QW})}{1 + \varepsilon * S} - \frac{S}{\tau_p} + \frac{\Gamma * N_{QW} * \beta}{\tau_{rad}} \tag{4}$$

Where τ_{bw} is the total carrier capture time from the barrier to QW; τ_{rad} is the radiative recombination lifetime in the QW, $\tau_{rad} = 1/(N_{QW} B)$; τ_{nonrad} is the non-radiative recombination lifetime determined by various effects such as Auger recombination, $\tau_{nonrad} = 1/(A + N_{QW}^2 C)$; τ_e is the carrier escape time from the QW to the barrier region; τ_b is the total recombination lifetime of the carriers in the barrier region; and τ_p is the photon lifetime, $\tau_p = 1/[v_g(\alpha_i + \alpha_m)]$. V_B is the volume of the barrier region, V_{QW} is the volume of the quantum well. Γ is the modal confinement factor, v_g is the group velocity of the mode, $g(N_{QW})$ is the peak gain provided by the carriers in the QW, ε is the intrinsic gain compression factor, and β is the spontaneous emission coupling to the lasing mode.

A. Steady-State At Threshold Condition

Here, only the threshold and below the threshold are considered. Therefore, the photon density S can be approximated to be zero. In the steady-state conditions, we can obtain:

$$N_B = \tau_{bw} * \frac{V_{QW}}{V_B}\left[N_{QW}\left(\frac{1}{\tau_e} + \frac{1}{\tau_{QW_total}}\right)\right] \tag{5}$$

$$\frac{I_{SCH}}{q} = N_B V_B * \left(\frac{1}{\tau_b} + \frac{1}{\tau_{bw}}\right) - \frac{N_{QW} V_{QW}}{\tau_e} \tag{6}$$

where τ_{QW_total} is the total recombination lifetime in the QW, $1/\tau_{QW_total} = 1/\tau_{rad} + 1/\tau_{nonrad}$. The barrier-well capture time τ_{bw} consists of the carrier transport time τ_r and the

quantum-capture time τ_{cap}, $\tau_{bw} = \tau_r + \tau_{cap}$ [30], [35], [36]. Due to the large electric field, the carrier transport near the quantum well follows the ambipolar carrier transport. The carrier transport time τ_r can be described as [37], [38]:

$$\tau_r = \frac{L_S^2}{2D_a} \tag{7}$$

here, L_S is the width of the undoped region in the confinement region. The ambipolar diffusion coefficient D_a is given by:

$$D_a = \frac{2D_n D_p}{D_n + D_p} \tag{8}$$

Where D_n and D_p are the diffusion coefficients of electrons and holes, $D_{n/p} = (kT/q)\mu_{n/p}$. Here, we have taken Hall mobility for electrons at room temperature in $Al_{0.4}Ga_{0.6}As$ to be 1000 cm^2/Vs and holes to be 80 cm^2/Vs [39], [40]. The temperature characteristics of mobility are assumed to be fitted by $(1/T)^2$[30]. Compared with the carrier transport time τ_r, the quantum-capture time τ_{cap} is negligible and can be disregarded [41].

B. Carrier Escape Time

The carrier escape time τ_e is very important for the analysis of dynamic and static performance of quantum-well laser. Here we use a simplified model, assuming that the transition of carriers between the unconfined and confined states are elastic, and thus neglecting the energy difference between the initial and final states [34]. Neglecting the influence of phonon energy and phonon number on the escape process, the escape current density can be expressed as:

$$J_e = qwn_L \frac{1}{4}\frac{m_c}{\pi\hbar^2}\left(\frac{2m_u kT}{\pi\hbar^2}\right)^{3/2} exp\left(-\frac{E_c^b - E_{fn}^c}{kT}\right) \tag{9}$$

where w is the constant related to the transition rate between a confined and an unconfined state, n_L is the number of electron-confined levels, $m_{c/u}$ is the effective mass of the confine/unconfined carriers, E_{fn}^c is the quasi-Fermi level for the confined carriers, and E_c^b is the energy of the edge of the barrier conduction band. The carrier escape time τ_e can be obtained from the escape current density J_e and the carrier density in the quantum well N_{QW}, $\tau_e = J_e/qN_{QW}$. It is assumed that only one confined level of electrons, the escape times τ_e can be obtained [30], [34], [42]:

$$\tau_e = 4\frac{kT}{w}\left(\frac{\pi\hbar^2}{2m_u kT}\right)^{3/2} * \frac{exp\left(\frac{qV_b}{kT}\right)}{1 + exp\left(\frac{E_{fn}^c - E_{0n}}{kT}\right)} \tag{10}$$

where qV_b is the energy difference between the first confined level and the edge of the barrier conduction band, and E_{0n} is the quantized energy levels of confined carriers. As shown in Fig 2, the relationship between escape time τ_e and temperature is calculated for barrier energy V_b of 130meV (red) and 160meV (bule) under carrier density of 1.9$*10^{18}\text{cm}^{-3}$ (solid) and 2.1$*10^{18}\text{cm}^{-3}$ (dashed) in quantum well. The carrier escape time decreases significantly with the increase of temperature, and the increase of barrier height can effectively inhibit the carrier escape.

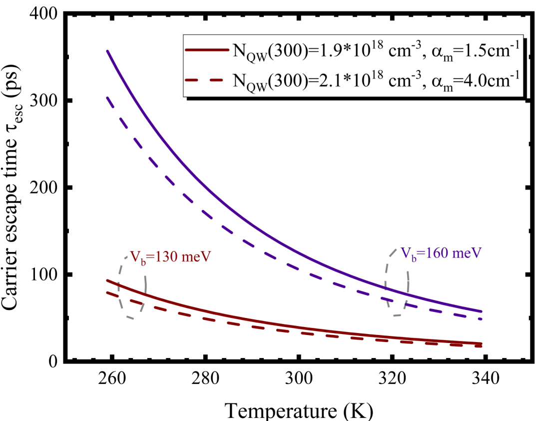

Fig. 2. Calculated carrier escape time τ_{esc} as a function of temperature.

C. Optical Gain and Internal Loss

Without considering the broadening, assuming only the first subband participates in the transition, the material gain can be expressed as [31]:

$$g_0^{\max} = I_{cv}^2 \frac{\pi}{L_{QW}}\frac{\alpha}{\sqrt{\epsilon}}\frac{M}{1+M}\left(1 - \frac{m_e}{m_0}\right)\frac{E_g(E_g + \triangle_0)}{E_g + \frac{2}{3}\triangle_0} \times \frac{1}{E_{\max}} \times \left(\left(exp\left(\frac{E_{0n} - E_{fn}^c}{T}\right) + 1\right)^{-1} + \left(exp\left(\frac{E_{0p} - E_{fp}^c}{T}\right) + 1\right)^{-1} - 1\right) \tag{11}$$

where I_{cv} is the overlap integral between the confined electron and hole envelope functions; L_{QW} is the quantum well width; $\alpha = q^2/\hbar c$; ϵ is the dielectric constant of the optical confinement layer; $M = m_h/m_e$, m_e and m_h are the electron and hole effective masses; m_0 is the free electron mass; E_g is the band gap and $\triangle_0$ is the energy of the spin-orbit splitting; $E_{\max}$ is the energy that the gain is at its maximum; $E_{0n/p}$ are quantized energy levels of an electron and a hole, $E_{fn/p}^c$ are the quasi-Fermi levels for the electrons and holes.

The carrier density in the quantum well can be expressed as:

$$N_{QW} = N_c ln\left(exp\left(\frac{E_{0n} - E_{fn}^c}{T}\right) + 1\right) \tag{12}$$

$$P_{QW} = N_v ln\left(exp\left(\frac{E_{0p} - E_{fp}^c}{T}\right) + 1\right) \tag{13}$$

The effective state density is linearly dependent on temperature, $N_{c/v} = m_{e/h}T/\pi\hbar^2$. the maximum gain can be expressed in terms of carrier densities as follows:

$$g_0^{\max} = I_{cv}^2 \frac{\pi}{L_{QW}}\frac{\alpha}{\sqrt{\epsilon}}\frac{M}{1+M}\left(1 - \frac{m_e}{m_0}\right)\frac{E_g(E_g + \triangle_0)}{E_g + \frac{2}{3}\triangle_0}\frac{1}{E_{\max}} \times \left(1 - exp\left(-\frac{N_{QW}}{N_c}\right) - exp\left(-\frac{P_{QW}}{N_v}\right)\right) \tag{14}$$

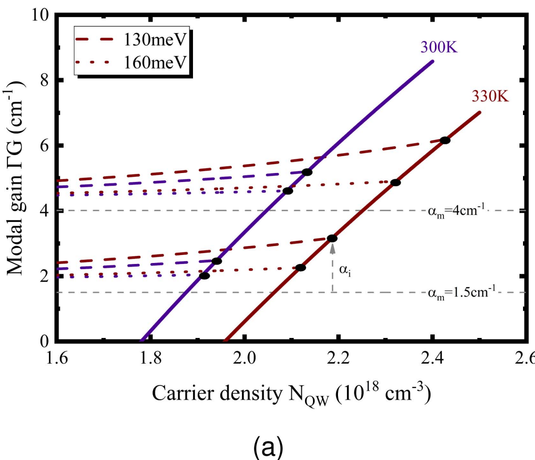

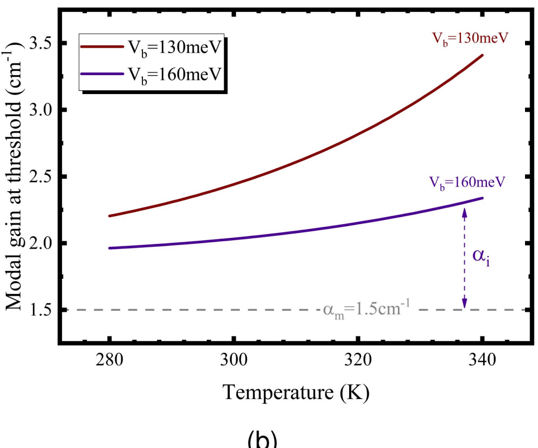

Fig. 3. (a) The maximum modal gain (solid) as a function of carrier density in quantum well N_{QW}; (b) Calculate the modal gain at threshold current various the temperature.

Suppose that the density of electrons and holes in quantum well is approximately equal, $N_{QW} = P_{QW}$. Assume now that $1 - exp(-N_{QW}/N_c) - exp(-P_{QW}/N_v) \propto ln(N_{QW}/N_{tr})$. Material gain can be expressed as a classical logarithmic function:

$$g_0^{\max} = G_{0N} ln(N_{QW}/N_{tr}) \tag{15}$$

As can be seen from the above formula, when the change of internal loss is negligible, the threshold carrier density N_{th} is approximately linearly correlated with temperature, $N_{th} \propto T$. The gain parameter G_{0N} has little relation with temperature.

The internal loss α_i can be expressed as the overlap integral of the fundamental mode and the carrier distribution, and the free carrier absorption of the waveguide is assumed to be linearly dependent on the carrier density in waveguide [5], [43]:

$$\alpha_i = \int \psi^2(x)(\sigma_n N_n(x) + \sigma_p N_p(x))dx$$
$$\approx \Gamma_{QW} c_{QW} N_{QW} + \Gamma_{WG} c_{WG} N_B + \Gamma_{clad}\alpha_{clad} \tag{16}$$

There, $\psi^2(x)$ is the normalized optical density; $N_n(x)$ and $N_p(x)$ are the carrier density at x position; σ_n and σ_p are the free carrier absorption coefficients of electrons and holes; c_{QW} and c_{WG} is the differential absorption coefficients of quantum well and waveguide. With the decrease of escape time τ_e, the carrier density in the waveguide N_B gradually increases, leading to an increase in internal loss α_i, As shown in Fig. 3(a). This means that the device requires a higher threshold carrier density to achieve the lasing condition. It is an obvious positive feedback process and leads to a sharp degradation of device performance under high threshold carrier density [5]. As shown in Fig. 3(b), due to the increase in internal losses, the modal gain required for laser emission increases with temperature, and the threshold carrier density cannot be simply considered to be linearly dependent on temperature [20].

D. Injection Efficiency

The current injection efficiency η_{inj} is different from the internal differential quantum efficiency η_i. The current injection efficiency is expressed as the ratio of the injected current in the active region to the total current, $\eta_{inj} = I_{QW}/I_{SCH}$. I_{QW} is the current injected into the active region:

$$I_{QW} = V_{QW} q \left(\frac{N_{QW}}{\tau_{QW_total}} + \frac{v_g * S * g(N_{QW})}{1 + \varepsilon * S}\right) \tag{17}$$

In a steady state, the generation rate of photons density is equivalent to the rate at which they are lost, therefore the internal differential quantum efficiency can be expressed as:

$$\eta_i = \frac{d(SV_{QW}/\tau_p\Gamma)}{d(I_{SCH}/q)} \tag{18}$$

Due to the threshold clamping effect, the internal differential quantum efficiency at the threshold is often higher than the electrical injection efficiency at the threshold.

For the below-threshold and at-threshold condition, the photon density in the cavity is typically minimal, the current injection efficiency of the quantum well can be expressed as follows [35]:

$$\eta_{inj_at_th} = \frac{1}{1 + \frac{\tau_{bw}}{\tau_b}(1 + \frac{\tau_{QW_total}}{\tau_e})} \tag{19}$$

The current injection efficiency in the active region is largely dependent on the recombination rate in the active region, with a faster recombination rate in the active region being more likely to achieve a higher current injection efficiency. The curve of calculated current injection efficiency with temperature variation is shown in Fig. 4(a). In the case of high potential barriers, the variation of current injection efficiency with temperature and threshold carrier density is not significant. As the barrier decreases, the correlation between injection efficiency and temperature and threshold carrier density becomes significantly higher.

Unlike the case below the threshold current, above the threshold current, the carrier density in the active region is clamped

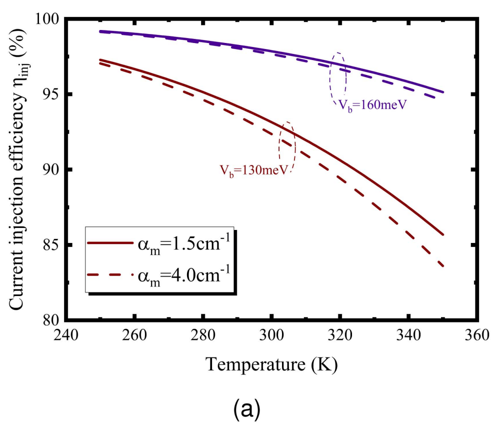

(a)

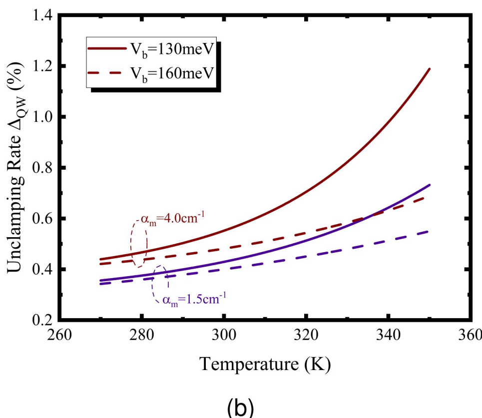

(b)

Fig. 4. (a) Current injection efficiency as function of temperature; (b) Unclamping rate $\triangle_{QW}$ various the temperature.

by the gain condition. At this time, the above-threshold current-injection efficiency $\eta_{inj_above_th}$ can be described as [35]:

$$\eta_{inj_above_th} = \frac{1 - \triangle_{QW} * \left(\frac{1}{\eta_{inj_at_th}} - \beta * \left(1 + \frac{\tau_{bw}}{\tau_b}\right)\right)}{1 + \frac{\tau_{bw}}{\tau_b}} \approx 1 - \frac{\triangle_{QW}}{\eta_{inj_at_th}} \tag{20}$$

In general, the value of β typically falls between 0.001 and 0.01, and the ratio τ_{bw}/τ_b is approximately 0.001, much smaller than unity [35], [36]. The unclamping rate $\triangle_{QW}$ is defined as the relative increase of the carrier density in the QW with injected current above threshold, $\triangle_{QW} = d(N_{QW}V_{QW}/\tau_{QW_total})/d(I_{SCH}/q)$. At low current, the unclamping rate does not change obviously with the current [44], [45]. It is assumed that the contribution of spontaneous radiation to photon density S can be ignored below the threshold current. By substituting (2)–(4), the unclamping rate $\triangle_{QW}$ can be expressed as follows:

$$\triangle_{QW} = 1 - \frac{d(N_B V_B/\tau_b)}{d(I_{SCH}/q)} - \frac{d(SV_{QW}/\tau_p\Gamma)}{d(I_{SCH}/q)} = 1 - \frac{dI_{leakage}}{dI_{SCH}} - \eta_i \tag{21}$$

Here, $I_{leakage}$ represents the leakage current caused by the recombination of carriers in barrier region. The unclamping rate $\triangle_{QW}$ is related to the carrier escape, and it significantly increases as the temperature and threshold carrier density increase, as shown in Fig. 4(b).

III. Experiment

The studied sample is a laser diode emitted at 780 nm. We adopt a 7 nm InAlGaAs material as a quantum well, with evident carrier leakage due to a smaller conduction band offset [3]. The waveguide layer is made of $Al_{0.4}Ga_{0.6}As$ material with a thickness of 1 μm, while the N-side waveguide has a thickness of 600 nm. The cladding layers on both sides are made of $Al_{0.65}Ga_{0.35}As$ material. The device is prepared using metal-organic chemical vapor (MOCVD) epitaxial growth technique and is further fabricated through photolithography to form single emitters with a length of 5 mm and a width of 100 μm[46]. The back facet of the device is coated with a high reflectivity film of 99.9%, while the front facet has a 1.5% antireflection film. By retaining the HR facet, uncoated devices with cavity lengths of 2 mm, 3 mm, and 4 mm are prepared through cleaving. All devices are packaged on AlN heat sink using the same packaging process. To test the device, pulse conditions are employed with a pulse width of 200us and a frequency of 50 Hz. At this time, the device does not exhibit significant temperature drift and thermal effects can be ignored. The device power curve is obtained through thermopile sensor (PM150-50C) testing, while the threshold current is determined by applying linear fitting on the low current power curve.

A. Threshold Current

Using a series of very restrictive assumptions including a parabolic two-band approximation with non-degenerate Maxwell–Boltzmann carrier distributions, the threshold current density of a semiconductor laser can be modeled using a semiempirical power law [20]:

$$J_{th}(N,T) = \frac{qL_{QW}}{\eta_{inj_at_th}}(AN + B(T)N^2 + C(T)N^3) \tag{22}$$

here, A is the monomolecular recombination coefficient associated with the defect states, B is the spontaneous radiative recombination coefficients, and C is the Auger recombination coefficients. In general, the current $J_{defect} = qL_{QW}AN$ depends mainly on the density of the defect state and can therefore be approximated as a constant [47]. The current due to spontaneous emission J_{spon} and Auger recombination J_{auger} is approximated by [48]:

$$J_{spon} = qL_{QW}B_0/TN^2 \tag{23}$$

$$J_{auger} = qL_{QW}C_0 exp\left(\frac{-E_a}{k_BT}\right)N^3 \tag{24}$$

The constants B_0 and C_0 are independent of temperature and carrier density. E_a is the empirical activation energy. For short-wavelength devices, due to their larger bandgap, they have a larger B_0 and smaller Auger recombination coefficient. Here, assume that the constant C_0 is equal to $5{*}10^{-28}cm^6/s$ and the

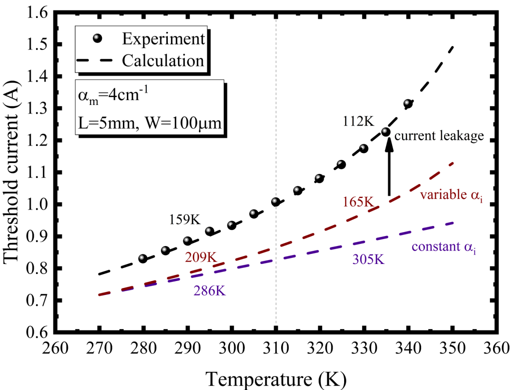

Fig. 5. Calculate and experiment the threshold current as a function of temperature.

activation energy E_a is equal to $170meV$. The Auger recombination current J_{auger} is much smaller than the spontaneous recombination current J_{spon}, where B_0=$3.4{*}10^{-10}$cm$^3/s$.

As shown in Fig. 5, the relationship between the threshold current and temperature change is depicted. The device is a coating device with a cavity length of 5 mm, corresponding to a mirror loss of $4cm^{-1}$. With the increase in temperature, the threshold current of the device significantly increases, and the temperature stability decreases as the temperature rises. The simulation results align well with the experimental findings. The threshold characteristic temperature of the device can be obtained by exponential fitting of threshold currents in different temperature ranges to account the super-exponential behavior of the characteristic temperatures. The threshold characteristic temperature T_0 is 159 K between 280 K to 310 K and 112 K between 310 K to 340 K. This is mainly due to the drastic deterioration of internal losses and injection efficiency.

When the internal losses and current inject efficiency variations with temperature are not taken into account, the device's threshold carrier density is considered to be linearly dependent on temperature, following the equation $N_{th} \propto T$, as mentioned previously. Under such circumstances, theoretically, the device should exhibit higher temperature stability, as indicated by the blue dashed line in Fig. 5. The threshold characteristic temperature exhibits an upward trend as the temperature rises. It reaches 286 K in the range of 280 K to 310 K, and further increases to 305 K within the range of 310 K to 340 K. This is consistent with the trend reported in the Ref [27]. Considering that the absorption loss varies with temperature, it is important to represent the threshold carrier concentration using a higher order temperature correlation function [20]. In this case, the threshold characteristic temperature decreases from 209 K to 165 K with increasing temperature, as depicted by the red dashed line in Fig. 5.

B. Transparency Current Density

Device transparent current density J_{tr} and modal gain coefficient ΓG_0 are usually obtained by linear fitting [47]:

$$ln(J_{th}) = ln\left(\frac{J_{tr}}{\eta_{inj}}\right) + \frac{1}{\Gamma G_0}(\alpha_i + \alpha_m) \tag{25}$$

The threshold current density under different cavity surface losses are obtained by pulse testing of devices with different cavity lengths, as shown in Fig. 6(a). Uncoated devices with cavity lengths of 2 mm, 3 mm, and 4 mm correspond to mirror losses of $1.5cm^{-1}$, $2cm^{-1}$, and $3cm^{-1}$, respectively. In Fig. 6(b), it can be observed that the fitted transparent current density gradually increases with temperature. With the rise in temperature, the fitted transparent current density shows an increase from $123A/cm^2$ at 280 K to $176A/cm^2$ at 340 K. The black dashed line represents the theoretically transparent current density that exhibits a linear correlation with temperature [47]. However, due to the obvious carrier leakage, the transparent current density obtained by fitting is higher than the actual value [49]. The simulated results, represented by the blue dashed line in Fig. 6(b), which calculated the threshold current density for different mirror losses under various temperature conditions and using the same method to linear fitted the threshold current density.

C. Threshold Characteristic Temperature

The threshold characteristic temperature at different temperatures can be obtained by exponential fitting of the threshold current density at different temperature ranges, as shown in Fig. 7(a). The threshold characteristic temperature decreases as the mirror loss of the device increases. For instance, at a temperature of 295 K, the threshold characteristic temperatures for mirror loss of $1.5cm^{-1}$, $2cm^{-1}$, $3cm^{-1}$, and $4cm^{-1}$ are 177 K, 172 K, 165 K, and 158 K, respectively. With the increase of temperature, the threshold characteristic temperature of the device decreases gradually, and the higher the mirror loss of the device, the more obvious the threshold characteristic temperature decrease [16].

To understand the contribution of different terms to the threshold characteristic temperature, the inverse ratio of the threshold characteristic temperature can be described as [47]:

$$\frac{1}{T_0} = \frac{1}{T_{tr}} + \frac{1}{T_{\eta_{inj}}} + \frac{\alpha_i + \alpha_m}{\Gamma G_0}\frac{1}{T_{G_0}} + \frac{\alpha_i}{\Gamma G_0}\frac{1}{T_{\alpha_i}} \tag{26}$$

the characteristic temperature of each item is described as:

$$\frac{1}{T_{tr}} = \frac{1}{J_{tr}}\frac{dJ_{tr}}{dT} \tag{27}$$

$$\frac{1}{T_{\eta_{inj}}} = -\frac{1}{\eta_{inj}}\frac{d\eta_{inj}}{dT} \tag{28}$$

$$\frac{1}{T_{G_0}} = -\frac{1}{G_0}\frac{dG_0}{dT} \tag{29}$$

$$\frac{1}{T_{\alpha_i}} = \frac{1}{\alpha_i}\frac{d\alpha_i}{dT} \tag{30}$$

In general, T_{G_0} is extremely large and therefore can be ignored [18]. The relationship between the inverse of threshold characteristic temperature and the temperature is shown in Fig. 7(b). At low temperatures, the escape of carrier escape is suppressed, and the threshold characteristic temperature of the device primarily depends on the transparent current density's characteristic temperature. With the increase of temperature, the

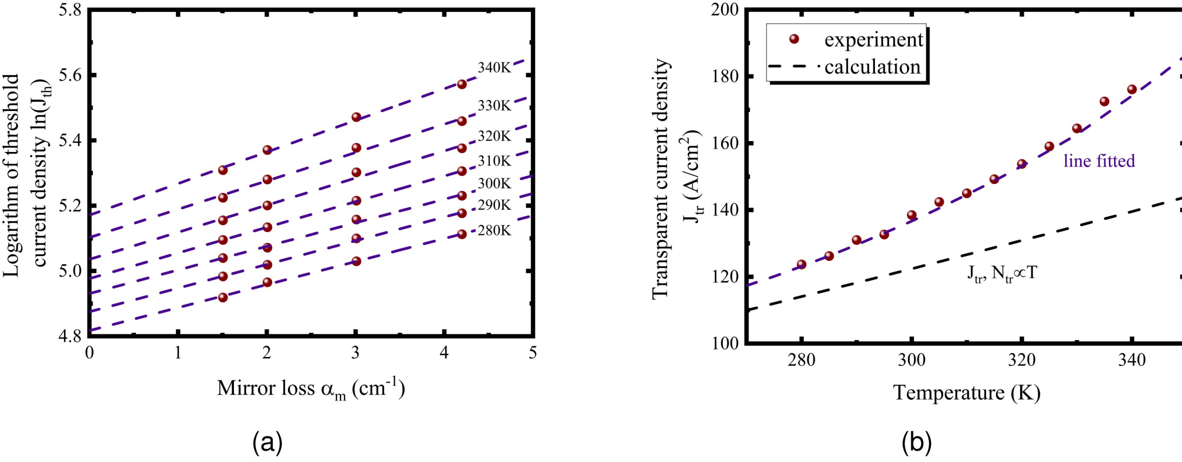

Fig. 6. (a) Natural logarithm of threshold current density versus mirror loss; (b) transparent current density at different temperatures.

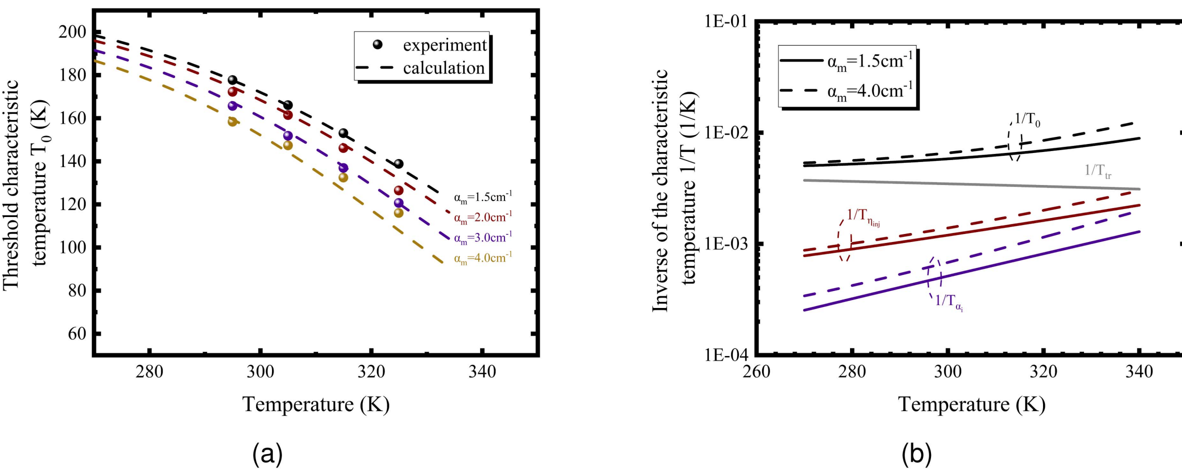

Fig. 7. (a) Threshold characteristic temperature as a function of temperature; (b) the contribution of different terms to the characteristic temperature.

transparent current density shows higher temperature stability. The carrier escape becomes more obvious, and the characteristic temperature corresponding to the internal loss and the electric injection efficiency deteriorates rapidly, resulting in the deterioration of the threshold characteristic temperature with the increase of temperature.

IV. Conclusion

The threshold temperature characteristics of short-wavelength laser diodes are simulated and analyzed using rate equations. In addition, the threshold temperature characteristics of devices with different mirror losses are compared. We utilize a simplified carrier escape model of quantum well, which is more accurate compared to the classical thermal carrier emission model. We consider the impact of carrier escape on internal losses, resulting in a more pronounced temperature dependence of the threshold carrier density. Furthermore, we analyze the temperature dependence of the unclamping rate, which significantly increases the temperature dependence of the internal quantum efficiency. The simulate threshold current density and threshold characteristic temperature are found to be similar to the experimental results, effectively explaining the phenomenon of the threshold characteristic temperature decreasing with increasing temperature. The increase internal losses and reduced injection efficiency caused by carrier escape are the main reasons for the temperature dependence of device characteristics decreasing with temperature. Notably, devices with higher thresholds are found to exhibit more pronounced characteristic temperature changes, as they are more susceptible to carrier escape. Increasing the barrier height is an effective means to suppress carrier escape and ensure stable operation of high threshold current density devices under high temperature conditions.

References

[1] M. S. Zediker and E. P. Zucker, “High-power diode laser technology XX: A retrospective on 20 years of progress,” *Proc. SPIE*, vol. 11983, 2022, Art. no. 1198302.
[2] B. Wang et al., “High reliability 808 nm laser diodes with output power over 19 W under CW operation,” *IEEE Photon. Technol. Lett.*, vol. 34, no. 6, pp. 349–352, Mar. 2022.

[3] B. Wang, L. Zhou, S. Tan, W. Liu, G. Deng, and J. Wang, “71% wall-plug efficiency from 780 nm-emitting laser diode with GaAsP quantum well,” *Opt. Laser Technol.*, vol. 168, 2024, Art. no. 109867.

[4] B. S. Ryvkin and E. A. Avrutin, “Asymmetric, nonbroadened large optical cavity waveguide structures for high-power long-wavelength semiconductor lasers,” *J. Appl. Phys.*, vol. 97, no. 12, 2005, Art. no. 123103.

[5] T. Kaul, G. Erbert, A. Maaßdorf, S. Knigge, and P. Crump, “Suppressed power saturation due to optimized optical confinement in 9xx nm high-power diode lasers that use extreme double asymmetric vertical designs,” *Semicond. Sci. technol.*, vol. 33, no. 3, 2018, Art. no. 035005.

[6] D. Botez, “Design considerations and analytical approximations for high continuous-wave power, broad-waveguide diode lasers,” *Appl. Phys. Lett.*, vol. 74, no. 21, pp. 3102–3104, 1999.

[7] D. Bour and A. Rosen, “Optimum cavity length for high conversion efficiency quantum well diode lasers,” *J. Appl. Phys.*, vol. 66, no. 7, pp. 2813–2818, 1989.

[8] J. Wang, B. Smith, X. Xie, X. Wang, and G. T. Burnham, “High-efficiency diode lasers at high output power,” *Appl. Phys. Lett.*, vol. 74, no. 11, pp. 1525–1527, 1999.

[9] H. Yu, S. Tan, H. Pan, S. Sun, J. Li, and J. Wang, “Development of a 350 W, 50 μm, 0.15 NA wavelength stabilized fiber coupled laser diode module for pumping Yb-doped fiber laser,” *Proc. SPIE*, vol. 11262, 2020, Art. no. 112620V.

[10] H. Yu, S. Tan, H. Pan, S. Sun, J. Li, and J. Wang, “High efficiency 600 W, 100 μm wavelength stabilized fiber coupled laser diode module for fiber laser pumping,” *Proc. SPIE*, vol. 11668, 2021, Art. no. 116680E.

[11] H. Yu et al., “High-brightness fiber-coupled diode module using dense wavelength beam combining technology based on single emitter for material processing and fiber amplifier pumping,” *Proc. SPIE*, vol. 11983, 2022, Art. no. 119830A.

[12] J. Pankove, “Temperature dependence of emission efficiency and lasing threshold in laser diodes,” *IEEE J. Quantum Electron.*, vol. 4, no. 4, pp. 119–122, Apr. 1968.

[13] T. Garrod et al., “50 diode lasers,” *Appl. Phys. Lett.*, vol. 105, no. 7, 2014.

[14] L. Bao et al., “Performance and reliability of high power 7xx nm laser diodes,” *Proc. SPIE*, vol. 7953, 2011, Art. no. 79531B.

[15] J. D. Evans, J. G. Simmons, D. A. Thompson, N. Puetz, T. Makino, and G. Chik, “An investigation into the temperature sensitivity of strained and unstrained multiple quantum-well, long wavelength lasers: New insight and methods of characterization,” *IEEE J. Sel. Topics Quantum Electron.*, vol. 1, no. 2, pp. 275–284, Jun. 1995.

[16] T. J. Houle, A. I. Onischenko, J. M. Rorison, R. V. Penty, and T. Garanzotis, “Temperature dependence of threshold current: A better criterion than t0 ?,” *Proc. SPIE*, vol. 4283, pp. 238–246, 2001.

[17] N. Tansu et al., “Temperature analysis and characteristics of highly strained InGaAs-GaAsP-GaAs ($\lambda > 1.17\mu m$) quantum-well lasers,” *IEEE J. Quantum Electron.*, vol. 38, no. 6, pp. 640–651, Jun. 2002.

[18] T. Higashi, T. Yamamoto, S. Ogita, and M. Kobayashi, “Experimental analysis of characteristic temperature in quantum-well semiconductor lasers,” *IEEE J. Sel. Topics Quantum Electron.*, vol. 3, no. 2, pp. 513–521, Apr. 1997.

[19] T. J. Houle et al., “Characterization of the temperature sensitivity of gain and recombination mechanisms in $1.3\mu m$ AlGaInAs MQW lasers,” *IEEE J. Quantum Electron.*, vol. 41, no. 2, pp. 132–139, Feb. 2005.

[20] J. Hader, J. V. Moloney, and S. W. Koch, “Temperature dependence of radiative and Auger losses in quantum wells,” *IEEE J. Quantum Electron.*, vol. 44, no. 2, pp. 185–191, Feb. 2008.

[21] D. Quandt, D. Arsenijević, A. Strittmatter, and D. H. Bimberg, “Static and dynamic characteristics of in (AsSb)/GaAs submonolayer lasers,” *IEEE J. Quantum Electron.*, vol. 55, no. 3, Jun. 2019, Art. no. 2000807.

[22] M. Asada and Y. Suematsu, “The effects of loss and nonradiative recombination on the temperature dependence of threshold current in 1.5-1.6 μm GaInAsP/InP lasers,” *IEEE J. Quantum Electron.*, vol. 19, no. 6, pp. 917–923, Jun. 1983.

[23] M. Asada, A. Adams, K. Stubkjaer, Y. Suematsu, Y. Itaya, and S. Arai, “The temperature dependence of the threshold current of GaInAsP/InP DH lasers,” *IEEE J. Quantum Electron.*, vol. 17, no. 5, pp. 611–619, May 1981.

[24] L. A. Coldren, S. W. Corzine, and M. L. Mashanovitch, *Diode Lasers and Photonic Integrated Circuits*. Hoboken, NJ, USA: Wiley, 2012.

[25] A. Haug, “Relations between the T 0 values of bulk and quantum-well GaAs,” *Appl. Phys. B*, vol. 44, pp. 151–153, 1987.

[26] S. Sweeney, D. Lock, and A. Adams, “Carrier recombination in InGaAs (P) quantum well laser structures: Band gap and temperature dependence,” in *Proc. AIP Conf. Proc.*, 2005, pp. 1545–1546.

[27] B. Witzigmann and M. S. Hybertsen, “A theoretical investigation of the characteristic temperature T_0 for semiconductor lasers,” *IEEE J. Sel. Topics Quantum Electron.*, vol. 9, no. 3, pp. 807–815, May/Jun. 2003.

[28] H. Zhao, G. Liu, J. Zhang, R. A. Arif, and N. Tansu, “Analysis of internal quantum efficiency and current injection efficiency in III-nitride light-emitting diodes,” *J. Display Technol.*, vol. 9, no. 4, pp. 212–225, Apr. 2013.

[29] M. Meneghini et al., “Thermal droop in III-nitride based light-emitting diodes: Physical origin and perspectives,” *J. Appl. Phys.*, vol. 127, no. 21, 2020, Art. no. 211102.

[30] R. Nagarajan, M. Ishikawa, T. Fukushima, R. S. Geels, and J. E. Bowers, “High speed quantum-well lasers and carrier transport effects,” *IEEE J. Quantum Electron.*, vol. 28, no. 10, pp. 1990–2008, Oct. 1992.

[31] L. Asryan et al., “Threshold characteristics of InGaAsP/InP multiple quantum well lasers,” *Semicond. Sci. Technol.*, vol. 15, no. 12, 2000, Art. no. 1131.

[32] S. Suchalkin et al., “Optical gain and loss in 3 μm diode “W” quantum-well lasers,” *Appl. Phys. Lett.*, vol. 80, no. 16, pp. 2833–2835, 2002.

[33] C.-Y. Tsai, C.-Y. Tsai, Y.-H. Lo, R. M. Spencer, and L. F. Eastman, “Nonlinear gain coefficients in semiconductor quantum-well lasers: Effects of carrier diffusion, capture, and escape,” *IEEE J. Sel. Topics Quantum Electron.*, vol. 1, no. 2, pp. 316–330, Jun. 1995.

[34] B. Romero, J. Arias, I. Esquivias, and M. Cada, “Simple model for calculating the ratio of the carrier capture and escape times in quantum-well lasers,” *Appl. Phys. Lett.*, vol. 76, no. 12, pp. 1504–1506, 2000.

[35] N. Tansu and L. J. Mawst, “Current injection efficiency of InGaAsN quantum-well lasers,” *J. Appl. Phys.*, vol. 97, no. 5, 2005, Art. no. 1052.

[36] R. Nagarajan and J. E. Bowers, “Effects of carrier transport on injection efficiency and wavelength chirping in quantum-well lasers,” *IEEE J. Quantum Electron.*, vol. 29, no. 6, pp. 1601–1608, Jun. 1993.

[37] G. Taylor and P. Claisse, “Transport solutions for the SCH quantum-well laser diode,” *IEEE J. Quantum Electron.*, vol. 31, no. 12, pp. 2133–2141, Dec. 1995.

[38] G. Taylor and S. Jin, “Revisions to” transport solution for SCH QW laser diodes,” *IEEE J. Quantum Electron.*, vol. 34, no. 10, pp. 1886–1889, Oct. 1998.

[39] A. Saxena, “Hall to drift mobility ratio in Ga1- xAlxAs alloys,” *Solid State Commun.*, vol. 39, no. 7, pp. 839–842, 1981.

[40] A. K. Saxena, “Intervalley scattering in Ga1- x Al x As alloys,” *J. Appl. Phys.*, vol. 52, no. 9, pp. 5643–5646, 1981.

[41] I. Esquivias et al., “Carrier escape time in GaAs/AlGaAs and InGaAs/GaAs quantum well lasers,” *Proc. SPIE*, vol. 2684, pp. 17–26, 1996.

[42] N. Tansu, J.-Y. Yeh, and L. J. Mawst, “Experimental evidence of carrier leakage in InGaAsN quantum-well lasers,” *Appl. Phys. Lett.*, vol. 83, no. 11, pp. 2112–2114, 2003.

[43] P. Brosson et al., “Experimental determination of carrier-induced differential loss in 2-section GaInAsP/InP laser-waveguide,” *Electron. Lett.*, vol. 24, no. 25, pp. 1623–1624, 1989.

[44] Z. N. Sokolova, N. A. Pikhtin, and L. V. Asryan, “Two-valued characteristics in semiconductor quantum well lasers,” *J. Lightw. Technol.*, vol. 36, no. 11, pp. 2295–2300, Jun. 2018.

[45] L. V. Asryan and S. Luryi, “Two lasing thresholds in semiconductor lasers with a quantum-confined active region,” *Appl. Phys. Lett.*, vol. 83, no. 26, pp. 5368–5370, 2003.

[46] J. Wang et al., “Volume manufacturing of high-power diode lasers using 6” wafers,” *Proc. SPIE*, vol. 11983, 2022, Art. no. 1198306.

[47] N. Tansu and L. J. Mawst, “Analysis temperature characteristics of highly strained InGaAs-GaAsP-GaAs ($\lambda > 1.17\mu m$) quantum well lasers,” *Proc. SPIE*, vol. 4646, pp. 302–312, 2002.

[48] G. P. Agrawal and N. K. Dutta, *Semiconductor Lasers*. Berlin, Germany: Springer Sci. & Business Media, 2013.

[49] M. Rosenzweig, M. Mohrle, H. Duser, and H. Venghaus, “Threshold-current analysis of InGaas-InGaaSp multiquantum well separate-confinement lasers,” *IEEE J. Quantum Electron.*, vol. 27, no. 6, pp. 1804–1811, Jun. 1991.